

# *p*-band stability of ultracold atom gas in anharmonic optical lattice potential with large energy scales

Mateusz Łącki

*Institute of Theoretical Physics, Jagiellonian University, Łojasiewicza 11, 30-348 Kraków, Poland*

Using an optical potential with subwavelength resolution in the form of sharp  $\delta$ -like peaks, potential landscapes are created with increased anharmonicity in placement of lattice band energies and more favorable energy scales. In particular, this makes the ultracold atom *p*-band gas more stable. The article outlines the details of the construction and discusses the *p*-band stability in canonical cosine optical lattice potential, double well potential, and a combination of a classical cosine potential with dark state peaked potential.

## I. INTRODUCTION

Optical lattices make a convenient and powerful setting for experimental study of many-body physics using ultracold atoms. An observation that such systems are described by Hubbard-type models [1], followed by a realization of the Mott insulator-superfluid quantum phase transition [2], led to numerous proposals and experiments with ultracold atoms [3].

One of the research directions was populating higher bands of optical lattices [4, 5] with the ongoing debate on stability of such systems. This was in part motivated by prospects to create interesting superfluid states, time reversal symmetry breaking [6, 7] or emergence of  $p_x + ip_y$  order [8, 9], or quantum Hall physics [10, 11].

In addition to theory proposals, questions of more practical significance have been raised – a problem of preparing gas in the excited bands [12–15] and the question of stability and lifetime of such a gas [4, 16–18].

Higher bands can also be populated by coherent resonant band coupling [12–14, 19]. When the coupling of *s* to *p* band is resonant, and presence of other bands can be disregarded, a synthetic-dimension two-leg ladder system, carrying flux  $\pi$  per ladder plaquette is created [20].

In the standard optical lattice, the collisional stability of the *p*-band e.g. is limited due to the fact that total energy of two particles in *p* band is often very close to the configuration where one particle is in *s* and the other in the *d* band. This process is off-resonant when the lattice band energies are anharmonic, leading to prolonged lifetime, as observed in the experiment [4, 21, 22].

Deviation from equal spacing between subsequent band *s, p, d, ...*, necessary for collisional *p*-band stability has to dominate other energy scales such as interaction strength or amplitudes of time-dependent fields. The latter can be lowered, this increasing the stability. The price to pay however is that it the main feature of the *p*-band gas would be its existence, with serious limits on simulable physics, given practical limits on coherence time of ultracold lattice systems. In short, the real solution should be in the direction of making energy levels in lattice systems more anharmonic, and the energy scales larger.

In [23, 24] a method of creating a potential in the form of a comb of subwavelength, few-nanometer wide peaks

was proposed. It carries bands with non-harmonic energies  $\sim n^2$ . Moreover subwavelength-width double well systems [25] allow large values of energy scales for hopping and interaction.

In this work we explore the effects the anharmonic level spacing has on collisional stability of *p*-band gas and on coherent resonant coupling of *s* and *p* bands. We are also study the energy scales for the parameters of tight-binding models describing motion of ultracold atom in such potentials.

In Section II we give the tight-binding description of an ultracold atom gas in few lowest Bloch bands, and discuss energy level arrangement of classical optical lattice potentials including the double well potential, subwavelength comb potential, and a combination of the two. In Section III we discuss the simulation of long-term depletion of the *p*-band by collisional interactions in case for all considered optical potentials. In Section IV, we study the creation of the synthetic-dimension two-leg ladder system in *s* and *p* band of a 1D lattice system, focusing on the achieved energy scales and the containment of the system. We provide summary and outlook in Section V.

## II. MULTIBAND DESCRIPTION OF THE ULTRACOLD ATOM GAS IN THE OPTICAL LATTICES

The gas of ultracold atoms of mass  $m_a$  in the periodic optical lattice potential  $V_{\text{opt.}}(r)$  is described in the second quantization by the Hamiltonian of the form [1]:

$$H = \int d^3r \hat{\psi}^\dagger(r) \left[ -\frac{\hbar^2}{2m_a} \nabla^2 + V_{\text{opt.}}(r) \right] \hat{\psi}(r) + \frac{g}{2} \int d^3r \hat{\psi}^\dagger(r) \hat{\psi}^\dagger(r) \hat{\psi}(r) \hat{\psi}(r) d^3r. \quad (1)$$

The  $g = \frac{4\pi a_s \hbar^2}{m_a}$  is the strength of two-particle collisional interactions by *s*-wave scattering with a scattering length  $a_s$ , tunable by Feshbach resonances [26]. Such a system can be effectively 1D, when a tight harmonic confinement  $m_a \Omega^2 (y^2 + z^2)/2$  in *y* and *z* is used. In the following Subsection II A we restate the multiband tight-binding description of (1). In II B we introduce all the considered 1D optical potentials, in II C grounds for stability

are outlined. In Subsections II D-II G we discuss the particular features of the four cases considered in this work.

### A. Tight binding description

The  $x$ -periodic potential,  $V_{\text{opt.}}(r) = V_{\text{opt.}}(x) + m_a \Omega^2 (y^2 + z^2)/2$  admits a family of quasiperiodic eigenfunctions  $B_k^\alpha(\vec{r}) = B_k^\alpha(x)H(y)H(z)$ ,  $B_k^\alpha(x+a) = B_k^\alpha(x)e^{ika/\hbar}$  for each band  $\alpha = 0, 1, 2, \dots$  to the eigenenergy  $E^\alpha(k)$ . The  $k \in [-\pi/a, \pi/a]$  is a quasimomentum,  $a$  is the lattice constant, and  $H(\cdot)$  is the harmonic potential ground state. The interval  $[-\pi/a, \pi/a]$  is a Brillouin Zone (BZ). For large enough  $\Omega$  the directions  $y, z$  add just a global energy shift, and can be neglected. In this work we will consider only  $V_{\text{opt.}}(x)$  which are smooth and have one or two minima in one potential period.

For isolated bands, for each lattice site  $x_n$ , exponentially localized Wannier functions  $W_n^\alpha(x)$  can be constructed under mild assumptions [27–29]. Specifically:

$$W_n^\alpha(x) = \int_{k \in \text{BZ}} B_k^\alpha(x) e^{i(\theta_k + kan)} dk,$$

where  $\theta_k$  is chosen to minimize the spatial variance of the Wannier functions [27–29].

When the Hamiltonian (1) is expressed in the basis  $W_k^\alpha(x)$ , the Multi-band Bose-Hubbard (MBH) Hamiltonian is obtained

$$H_{\text{MBH}} = - \sum_{\alpha, n, m} J_{nm}^{\alpha\alpha} (\hat{a}_n^\alpha)^\dagger \hat{a}_m^\alpha + H.c. + \frac{1}{2} \sum_{\substack{\alpha \dots \delta \\ n \dots p}} U_{nmop}^{\alpha\beta\gamma\delta} (\hat{a}_n^\alpha)^\dagger (\hat{a}_m^\beta)^\dagger \hat{a}_o^\gamma \hat{a}_p^\delta, \quad (2)$$

where:

$$J_{nm}^{\alpha\alpha} = - \int dx W_n^\alpha(x) \left( -\frac{\hbar^2}{2m} \nabla^2 + V_{\text{opt.}}(x) \right) W_m^\alpha(x) \quad (3)$$

$$= \int_{\text{BZ}} e^{i(n-m)ka} E^\alpha(k) dk, \quad (4)$$

and

$$U_{nmop}^{\alpha\beta\gamma\delta} = g \int d\vec{r} W_n^\alpha(\vec{r}) W_m^\beta(\vec{r}) W_o^\gamma(\vec{r}) W_p^\delta(\vec{r}). \quad (5)$$

In particular,  $J_{nn}^{\alpha\alpha} \equiv \bar{E}_n^\alpha$  is the on-site energy of a particle at site  $n$  and band  $\alpha$ . The  $J_{n,n+1}^{\alpha\alpha} \equiv J^\alpha$  is nearest-neighbor hopping rate. In the formula for integrals  $U_{nmop}^{\alpha\beta\gamma\delta}$ , an integral of  $H^4(y)H^4(z)$  over  $y, z$  directions gives an overall factor that is incorporated in  $g$ .

When the gas populates the  $p$ -band, the full model (2) reduces to a single band Bose-Hubbard model,

$$H = -J \sum_{\langle n, m \rangle} (\hat{a}_n^\dagger \hat{a}_m + H.c.) + \sum_m \frac{U}{2} \hat{n}_m (\hat{n}_m - 1), \quad (6)$$

where  $U = U_{nnnn}^{1111}$ ,  $J = J_{n,n+1}^{11} = J^1$ . The model exhibits superfluid-Mott insulator quantum phase transition which occurs for  $J/U \approx 0.3$  [2, 30–34].

### B. Optical potentials

For ultracold atoms arbitrary optical potentials can be created using either stroboscopic projection schemes [35] or spatial light modulators [36–38]. Such techniques, however, imply either short system lifetime or relatively long lattice constants  $a \gg \lambda/2$  and in turn overall low energy scale for lattice dynamics given by the recoil energy  $E_R = \frac{\hbar^2}{8ma^2}$ .

The potential created by the AC-Stark shift due to a standing-wave field far detuned from an optical transition is of the form

$$V_{\text{latt}}(x) = V_x \cos^2 kx, \quad k = 2\pi/\lambda \quad (7)$$

where  $\lambda$  is the laser wavelength. By using two laser wavelengths a double-well potential is obtained:

$$V_{dw}(x) = V_2 \cos^2(k_2 x) + V_1 \cos^2(k_1 x + \phi), \quad k_1 = \frac{k_2}{2}. \quad (8)$$

We do not investigate a plethora of models where  $k_1 \neq k_2/2$  including but not limited to disordered systems [39].

Recently a scheme, based on coherent dark-state of atomic  $\Lambda$  system has been proposed [23, 24] that allows to create comb potentials of the form: with

$$V_{na}(\epsilon, x) = E_R \frac{\epsilon^2 \cos^2 kx}{(\epsilon^2 + \sin^2 kx)^2}, \quad (9)$$

where  $\epsilon \ll 1$  [see also Fig.3(a)].

The fourth class considered in this work is the combined potential

$$V_{\text{comb}}(x) = V_{na}(x) + V_{\text{latt}}(x). \quad (10)$$

All the above potentials share a common feature that the unit cell contains one or two potential minima. Then the low lying bands  $s, p, d \dots$  are *generally* simple, single-valued bands separated by a nonzero gap. The notable exception is the double well potential when  $V_1/V_2 \approx 0$  or  $V_2/V_1 \approx 0$ . Then the  $p$  and  $s$  band become almost degenerate.

### C. $p$ -band separation

A possible loss mechanism is when two colliding particles in the  $p$ -band end up in different bands: one in  $s$ -band and one in  $d$ -band. This process may be (nearly) resonant, when the wells of  $V_{\text{opt.}}(x)$  are well approximated by a harmonic potential.

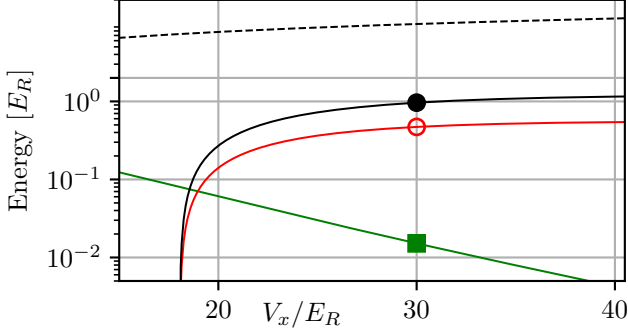


Figure 1. Figure shows the value of  $f$  (black curve, marked with full circle),  $\Delta_{sp}$  (black dashed line), and  $U^{1111}$  (red solid line, marked with empty circle) assuming  $U^{1120} = f/10$ ,  $J^1$  (green curve, marked with a full square), for the classical optical potential  $V_{\text{latt}}$  as the function of its height  $V_x$  – see Eq. (7).

Let us consider two particles in the  $p$ -band with the total noninteracting energy in the interval  $\mathcal{A} = [2 \min E^1(q), 2 \max E^1(q)]$  and consider interaction-driven population of the final state with noninteracting energy in  $\mathcal{B} = [\min E^0(q) + \min E^2(q), \max E^0(q) + \max E^2(q)]$ . The process  $p+p \rightarrow s+d$  is not resonant only if the distance between intervals  $\mathcal{A}$  and  $\mathcal{B}$  is much larger than the interaction-induced coupling, namely when

$$f \equiv \text{dist}(\mathcal{A}, \mathcal{B}) \approx ||2\bar{E}^1 - \bar{E}^0 - \bar{E}^2| - 2|2|J^1| + |J^0| + |J^2||| \gg U_{nnnn}^{1120}. \quad (11)$$

The ratio  $f/U_{nnnn}^{1120}$  thus quantifies the extent to which the description of  $p$ -band gas given by (6) is valid. At the same time one desires that the parameters  $U, J$  in (6) are as large as possible in the absolute terms to make the system stable against thermal fluctuation. Additionally the time-scales defined by the model should be within coherence time of possible experimental setups.

In the forthcoming Sections we study in energy scales and the parameter  $f$  of the four potentials mentioned in Section II B.

#### D. Standard optical lattice potential

The low-energy sector of a Hamiltonian [Eq. (1)] describing a particle in the lattice potential  $V_{\text{latt}}(x)$  [Eq. (7)] for  $V_x \gg E_R$  resembles a system with a series of almost-decoupled nearly-harmonic traps. Taking into account quartic terms in expansion of  $\cos^2$  potential around its minima gives an approximate formula for  $n$ -th band energy:

$$E_n \approx \left(n + \frac{1}{2}\right) \sqrt{4V_x E_R} - \frac{6n^2 + 6n + 3}{12} E_R. \quad (12)$$

We note that in  $V_x \rightarrow \infty$  limit the quartic contribution is non-vanishing. The  $f$  defined in Eq. (11) for very large

$V_x \gg E_R$ , when all the hopping rates  $J^0, J^1, J^2$  are exponentially suppressed is therefore:

$$f \approx 2E_1 - E_0 - E_2 \rightarrow 1E_R \quad (13)$$

It is important to stress that the limit value in Eq. (13) is nonzero solely due to the quartic term in Eq.(12).

Specifically the  $f$  is nonzero [see Fig. 1] for  $V_x \gtrsim 18E_R$ . At around  $V_x \approx 30E_R$ ,  $f$  reaches  $1E_R$ . The maximum value of  $f$  is attained near  $V_x \approx 40E_R$  where  $f \approx 1.4E_R$ . Increasing the lattice height  $V_x$  and therefore  $f$  comes at the price of decrease of  $J^1$ . For  $V_x \approx 30E_R$  ( $40E_R$ ) we have  $J^1 \approx 0.015E_R$  ( $0.0042E_R$ ).

These  $p$ -band hopping rates are quite small. For a popular atom species used often in experiments, the  $^{87}\text{Rb}$ , typical parameters of lasers, the hopping frequency would be of the order of few tens of Hertz.

#### E. “Double-well” potential

By using two lasers one can create, by an AC-Stark shift a potential of the form (8). It has been used in countless theoretical and experimental works (just a few examples being [40–44]).

The double-well potential  $V_{dw}$  has a fundamental period twice larger than  $V_{\text{latt}}(x)$ , namely  $a = \lambda$ . When  $\phi = 0$  the potential is symmetric with respect to the center of the properly chosen unit cell  $x_0$  [see Fig. 2(a)]. The Wannier functions of  $s, p, d \dots$  band are then alternately even and odd with respect to the  $x_0$ . For  $V_2 \leq V_1/4$  the potential remains unimodal within the unit cell with minimum at  $x_0$ . At exactly  $V_1 = V_2/4$  at  $\partial_{xx} V_{dw}(x_{\min}) = 0$ , and the potential around the minimum is well-approximated by a quartic potential [see Fig. 2(a)]. For larger  $V_2$  there are two minima and the  $s$  to  $p$  band gap is significantly reduced.

The Fig. 2(b) shows the dependence of factor  $f$  as a function of  $V_2$  for fixed  $V_1 = 10E_R$  (solid lines) and  $V_1 = 20E_R$  (dashed lines). We see that for  $V_2 \approx V_1/4$  the factor  $f$  is  $0.35E_R$  for  $V_1 = 10E_R$  and  $f \approx 0.65E_R$  for  $V_2 = 20E_R$  the values of  $f$  reached are not larger than those achievable for the standard optical lattice ( $f \leq 1.4E_R$ ). This is primarily due to twice larger period of the unit cell. As a result the increased anharmonicity due to the dominant quartic term is scaled down by factor 4,  $E'_R = \frac{\hbar^2}{8ma^2} = \frac{E_R}{4}$ ,  $a = \lambda$ . The value of  $f$  can be increased by increasing both  $V_1$  and  $V_2$ . For fixed  $V_2 = V_1/4$ , in the limit of very large  $V_1, V_2$  the factor  $f$  can be arbitrarily large (in contrast to the  $V_{\text{latt}}$ ). The price to pay is the exponential decay of  $J^1$ , which for  $V_1 = 10E_R$  is  $O(10^{-3}E_R)$  and for  $V_1 = 20E_R$  is  $O(10^{-5} \div 10^{-4}E_R)$ . Increasing just  $V_2$ , while formally leading to the increase of  $f$ , actually leads to the degeneration of  $p$  and  $s$  band.

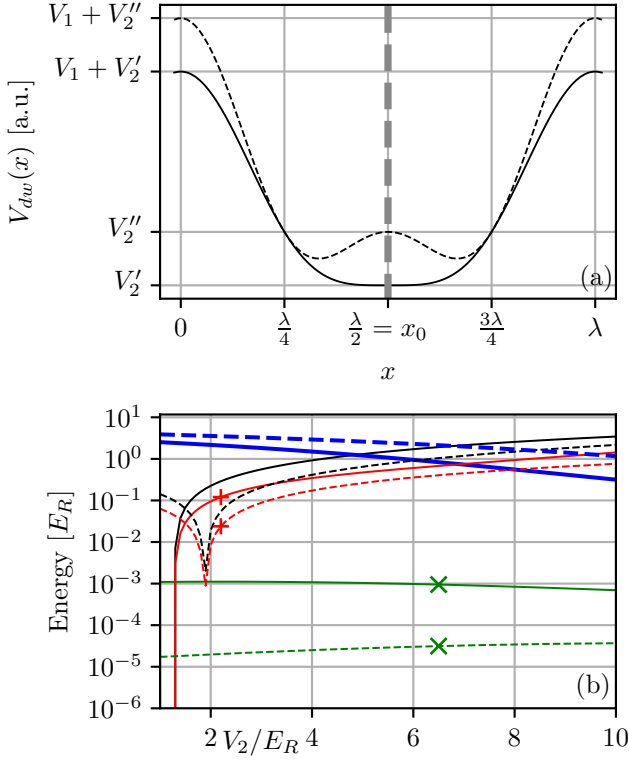


Figure 2. Figure shows the properties of the potential  $V_{dw}$ . Panel (a) parallels the discussion of the potential shape and symmetry in the main text; the vertical dashed gray line shows the symmetry axis. Solid line shows  $V_{dw}$  for  $V_2 = V_2' = V_1/4$ . Dashed line shows  $V_2 = V_2'' = V_1/2$  case. Panel (b) shows the value of  $f$  (black curve),  $\Delta_{sp}$  (blue, thick line), and  $U^{1111}$  (red with a '+'),  $J^1$  (green with a 'x') assuming  $U^{1120} = f/10$ , for the two-well optical potential  $V_{dw}$  as the function of  $V_2$  with  $V_1 = 10E_R$  (solid lines) or  $V_1 = 20E_R$  (dashed lines). See Eq. (8).

### F. Comb potential

The potential  $V_{na}(x)$  as given by Eq. (9) is achieved by preparing atoms in the three level system [23]:

$$H_c = -\frac{\hbar^2}{2m_a}\partial_x^2 + H_\Lambda(x), \quad (14)$$

where

$$H_\Lambda(x) = \hbar \begin{pmatrix} 0 & \Omega_c(x)/2 & 0 \\ \Omega_c(x)/2 & -\Delta - i\Gamma/2 & \Omega_p/2 \\ 0 & \Omega_p/2 & 0 \end{pmatrix} \quad (15)$$

has been written in the atomic level basis  $|g_1\rangle, |e\rangle, |g_2\rangle$ . The Rabi frequency  $\Omega_c(x)$  is a standing wave,

$$\Omega_c(x) = \Omega_c \sin[k(x - x_0)], \quad (16)$$

$\Omega_p$  is  $x$ -independent, and  $\epsilon = \Omega_p/\Omega_c$ . The position-dependent eigenstates of  $H_\Lambda(x)$  include the dark state

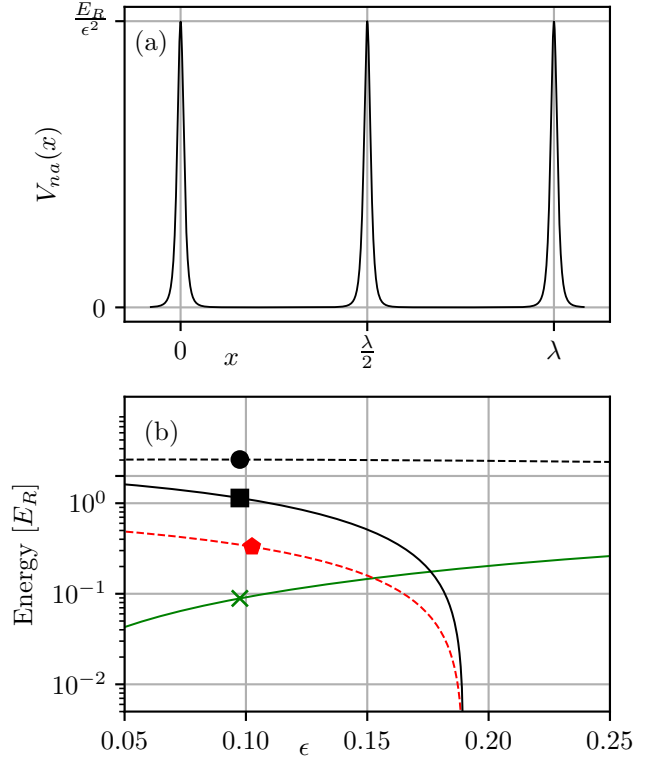


Figure 3. Figure shows the properties of the potential  $V_{na}$ . Panel (a) presents the shape and height of a potential  $V_{na}$  parametrized by  $\epsilon$ . Panel (b) shows the value of  $f$  (black curve with a square),  $\Delta_{sp}$  (black dashed line with a circle), and  $U^{1111}$  (red dashed line with a pentagon),  $J^1$  (green with a cross) assuming  $U^{1120} = f/10$ , for the comb optical potential  $V_{na}$  as the function dimensionless parameter  $\epsilon$  – see Eq. (9).

$|f_1(x)\rangle = -\cos\alpha(x)|g_1\rangle + \sin\alpha(x)|g_2\rangle$  with  $\alpha(x) = \arctan[\Omega_c(x)/\Omega_p]$ . It is an eigenstate to the zero energy for all  $x$ . There are also two right-orthonormal bright states  $|f_2(x)\rangle, |f_3(x)\rangle$ , eigenstates to nonzero energies  $E_{2,3}(x)$ . The set  $\{|f_n(x)\rangle\}_{n \in \{1,2,3\}}$  can be used as a new basis [23].

The restriction of  $H_c$  to the wavefunctions of the form  $g(x)|f_1(x)\rangle$  is given by:

$$H = -\frac{\hbar^2}{2m_a}\partial_x^2 + V_{na}(x), \quad (17)$$

In general subspace of the full Hilbert space spanned states of the form  $g(x)|f_1(x)\rangle$  for any  $g(x)$  is not invariant by the action of  $H_c$ : the dark states get coupled to both bright states. However, when  $\sqrt{\Omega_p^2 + \Omega_c^2(x)} \gg \Delta, \Gamma$ ,  $\sqrt{\Omega_p^2 + \Omega_c^2(x)} \gg E_R/\epsilon^2$  then wavefunctions  $\psi_D(x) = g(x)|f_1(x)\rangle$  with “small”  $\langle\psi_D|H_c|\psi_D\rangle$  form a nearly invariant subspace [23]. In another words, low energy sector of Eq. (17) describes well a part of the spectrum of the full  $H_c$ .

The potential  $V_{na}$  has the form of sharp potential peaks

[see 3(a)] of height  $E_R/\epsilon^2$  and width  $\sim \epsilon\lambda/2\pi$ , located at  $x = n\lambda/2, n \in \mathbb{Z}$ .

When  $\epsilon \rightarrow 0$  the potential peaks can be replaced by  $\frac{\pi}{2\epsilon} \sum_n \delta(x - n\lambda/2)$ . In that limit, mean band energies converge to values characteristic for a box potential,  $\bar{E}_n \approx n^2 E_R$ . It may be shown that the bandwidths of each band  $\Delta E_n \approx 4J^n \sim n^2 \epsilon E_R$  [see [23]].

The potential  $V_{na}$  allows to reach similar values of  $f$  as the standard optical lattice  $V_{\text{latt}}$  ( $f \approx 1.4E_R$  for  $\epsilon = 0.05$ , and  $f \approx 1E_R$  for  $\epsilon = 0.1$ ) [see Fig. 3(b)]. The anharmonicity of the mean band energies is  $|2\bar{E}_p - \bar{E}_s - \bar{E}_d| \approx 2E_R$  but only for very small  $\epsilon \approx 0$ , the hopping  $J^0, J^1, J^2$  is suppressed. Experiments conducted to this date operated with values of  $\epsilon \geq 0.05$ .

The values of hopping amplitude  $J^1$  for  $\epsilon \geq 0.05$  are actually order of magnitude larger than  $J^1$  for  $V_{\text{latt}}$  for same value of  $f$  ( $J^1 \approx 0.09E_R$  for  $\epsilon = 0.1$ , and for  $\epsilon = 0.05$  it is  $J^1 \approx 0.042E_R$ ). In contrast to  $V_{\text{latt}}$  it is challenging to significantly reduce  $J^1$  as the the potential barrier height  $\sim \epsilon^{-2}$  increased with  $\epsilon$  is partially compensated by its decreasing width  $\sim \epsilon$ . In the subwavelength comb the  $s$  to  $p$  and  $s$  to  $d$  band separations are almost  $\epsilon$ -independent and  $\Delta_{sp} \approx 3E_R, \Delta_{pd} \approx 5E_R$ .

The lifetime of the system implementing the  $V_{na}$  potential may also be overall limited [23, 24]. Use of atoms with trivial hyperfine structure would be a possible solution to the issues raised with first experiments. It should be also noted that the above  $\Lambda$  system has not been so far experimentally realized with the bosonic species.

### G. Classical potential together with the comb potential

Another possibility is opened by a combined potential that includes both a standard lattice potential  $V_{\text{latt}}$  and the  $V_{na}$  potential (parameter  $\phi$  allows for shift of  $V_{na}$  peak with respect to the minimum of  $V_{\text{latt}}$ ):

$$V_{\text{comb}}(x) = V_{\text{latt}}(x) + V_{na}(\epsilon, x - a\phi), \quad a = \lambda/2 \quad (18)$$

The combined potential  $V_{\text{comb}}(x)$  can be achieved when in Eq. (15) atoms in either of states  $g_1$  and  $g_2$  feel an additional, standard lattice potential due to AC-Stark shift, namely when the three-level Hamiltonian is of the form [24].

$$H_\Lambda(z) = \hbar \begin{pmatrix} V_1 \sin^2(kx) & \Omega_c(x - a\phi)/2 & 0 \\ \Omega_c(x - a\phi)/2 & -\Delta - i\Gamma/2 & \Omega_p/2 \\ 0 & \Omega_p/2 & V_1 \sin^2(kx) \end{pmatrix}.$$

The potential  $V_1 \sin^2(kx)$  is then simply added to  $V_{na}(x - a\phi)$  resulting in the desired  $V_{\text{comb}}(x)$ .

In the pure  $V_{\text{latt}}(x)$  potential the Wannier functions are alternately even and odd w.r.t to the center of the unit cell. A sharp potential in the middle of the cell, would primarily shift energies of each band, by a value  $\int_{\mathbb{R}} V_{na}(x) |W^\alpha(x)|^2 dx \approx \pi |W(0)|^2 / (2\epsilon)$ . The integral is

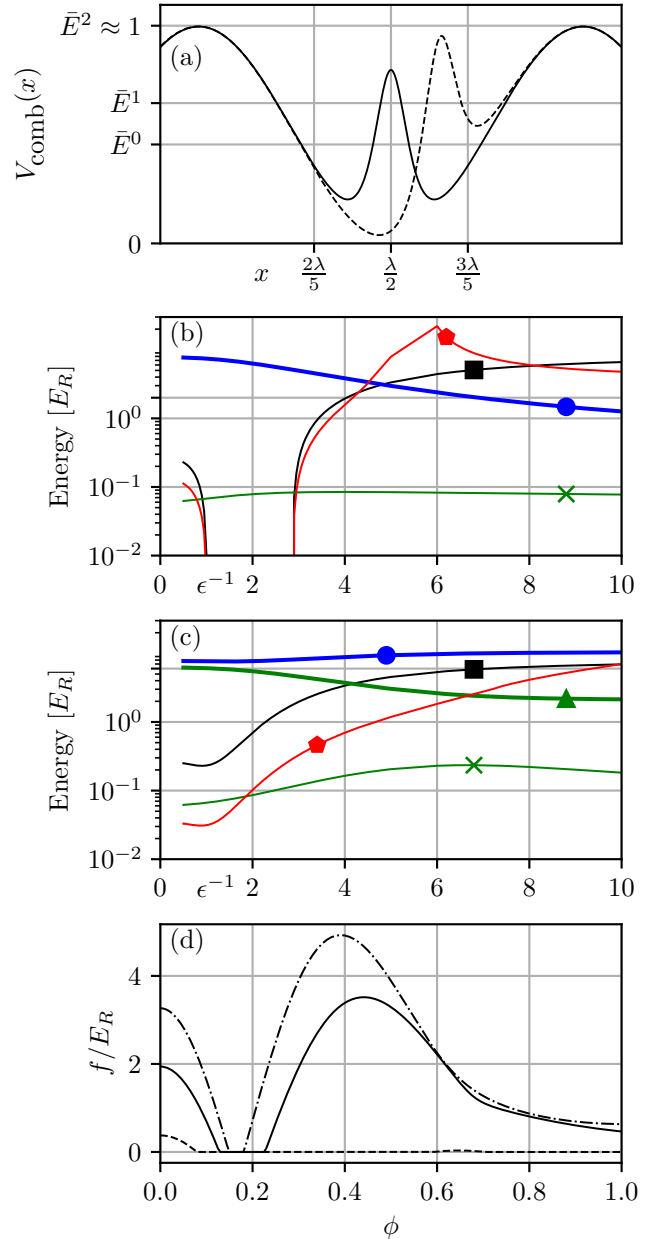


Figure 4. Properties of  $V_{\text{comb}}$ . Panel (a) shows the potential shape, around the potential minimum for  $V_x = 20E_R$ ,  $\epsilon = 0.25$  and  $\phi = 0$  (black solid line),  $\phi = 0.4/\pi$  (black dashed line). The levels  $\bar{E}^0, \bar{E}^1, \bar{E}^2$  indicate first three band energies for  $\phi = 0$ . Panels (b) and (c) show the value of  $f$  (black curve with a square),  $\Delta_{sp}$  (blue, thick line with a filled circle),  $\Delta_{pd}$  (green, with a triangle pointing up), and  $U^{1111}$  (red with a pentagon),  $J^1$  (green with a cross) assuming  $U^{1120} = f/10$ , for the combined optical potential  $V_{\text{comb}}$  (comb potential and classical  $\sin^2$  potential) as the function of dimensionless parameter  $\epsilon$  controlling the height of the comb potential with  $V_x = 10E_R$  [panel (b)] or  $V_x = 20E_R$  [panel (c)]. See Eq. (8). Panel (d) shows  $f/E_R$  for  $V_x = 10, 20, 30E_R$  and  $\epsilon^{-1} = 4$  (dashed, solid, dash-dotted black line) as a function of a shift  $\phi$  of subwavelength peak w.r.t to the potential minimum.

maximal for the  $s$ -band Wannier functions, and decays for subsequent even Wannier functions. It is zero for odd bands, including the  $p$ -band. As the anharmonicity, for deep lattice is given by  $f \approx 2\bar{E}^1 - \bar{E}^0 - \bar{E}^2 > 0$ , adding the central  $V_{na}$  peak should first lower the  $f$  first towards zero. Only after that the  $f$  can attain, large negative values.

Non-central placement of the  $V_{na}(\epsilon, x)$  offers more flexibility in manipulating the  $f \approx 2\bar{E}^1 - \bar{E}^0 - \bar{E}^2$  (see also [25]). For example, when the subwavelength peaks  $V_{na}$  coincide with maxima of the  $p$ -band Wannier function of  $V_{latt}(x)$  one can expect the mean  $\bar{E}^1$  to increase strongly in contrast to  $\bar{E}^0$  and  $\bar{E}^2$ . As a result the band anharmonicity should be increased to large positive values.

In Fig. 4(a) shows the parameters describing the properties of the  $V_{comb}$  for  $\phi = 0$  and for  $\phi = 0.4/\pi$ . In the latter case  $V_{na}(x - a\phi)$  nearly coincides with maximum of the  $p$ -band Wannier function.

When  $\phi = 0$  it is evident that the values of  $f$  that easily achieve value of  $f = 2E_R$  (for  $\epsilon \approx 0.25$ ) before, for even smaller  $\epsilon$ , the central peak given by  $V_{na}$  cuts the potential well into two almost disconnected parts, with tiny  $\Delta_{sp}$ . For  $\phi = 0$  we focus on  $\epsilon \approx 0.25$  when the  $\bar{E}^1$  is similar to the  $V_{na}$  peak height, the Wannier function of the  $p$  band is not strongly affected by the potential peak and  $\Delta_{sp}$  remains sizable.

For small  $\epsilon^{-1}$  the potential  $V_{comb}$  can resemble the potential  $V_{dw}$ . The crucial difference is that its period remains  $a = \lambda/2$  in contrast to period  $\lambda$  of  $V_{dw}$ . This allows to maintain much higher hopping rate in  $V_{comb}$ .

When  $\phi = 0.4/\pi$  the values of  $f$  that are reached are similar, with important difference: the value of  $f = 2\bar{E}^1 - \bar{E}^0 - \bar{E}^2$  for  $\epsilon^{-1} \rightarrow 0$  does not change the sign as  $\epsilon^{-1}$  is increased. This means that in contrast to  $\phi = 0$ , also for  $\epsilon^{-1} \leq 3$  the  $f$  is nonzero. This is important for practical applications as the spontaneous emission losses quickly grow with  $\epsilon^{-1}$  (see [23, 24]).

For all considered  $\phi$  the hopping rate  $J^1 \approx 0.1 \div 0.15E_R$ . It is half of the order of magnitude larger than for  $V_{latt}$  of the same potential height. This is simply due to the fact that putting extra potential  $V_{na}$  in the potential well makes it effectively shallower. In contrast to using a standard optical lattice  $V_{latt}$  working with the value of  $f \approx 1 - 2E_R$  requires  $V_x = 15 \div 20E_R$  while for  $V_{latt}$  the  $f \approx 1 - 1.4E_R$  is reached for deep lattices of  $V_x = 30 \div 40E_R$  with  $J^1$  hopping rate significantly reduced. At such value of  $\epsilon$  the combined potential retains workable features of the  $V_{latt}$  such as sizable  $\Delta_{sp} \approx 3.8E_R$ .

### III. COLLISIONAL STABILITY OF P-BAND CONDENSATE

In this section we numerically study the stability of the  $p$ -band gas in the potentials from the previous Section II. To this end we consider a small, strongly interacting system consisting of  $L = 2 - 4$  sites described by Hamilto-

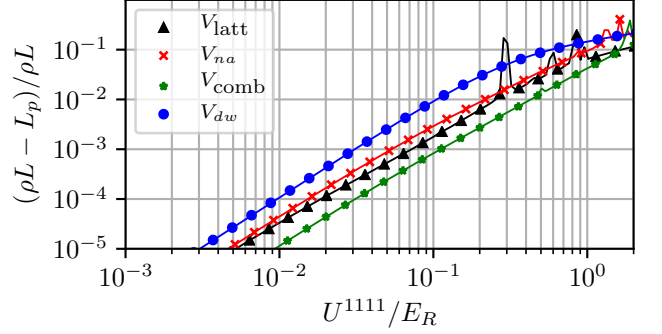


Figure 5. Mean losses from the  $p$ -band population of an interacting system for the four considered potentials, in a system of length  $L = 4$  populated with  $\rho L = 5$  particles.

nian  $H$  in Eq. (2) under periodic boundary conditions, restricted to lowest three bands.

As discussed in Sections IID-II G the four potentials considered in this work are characterized by very different values of  $J^1$ ,  $U^{1111}$  and the values of  $f$  one work with. For each of the four potentials we pick a single parameter set that is a compromise between maximizing the value of  $f$  and ease of realizability.

Specifically, we consider (we denote  $u = U^{1111}/U^{0000}$ ):

1. Potential  $V_{latt}$  of height  $V_x = 30E_R$  with  $f \approx 1E_R$  and:

$$(J^0, J^1, u) \approx (-0.00046E_R, 0.015E_R, 0.698), \quad (19)$$

2. Potential  $V_{na}$  for  $\epsilon = 0.1$  with  $f \approx 1.11E_R$  and:

$$(J^0, J^1, u) \approx (-0.022E_R, 0.091E_R, 0.985), \quad (20)$$

3. Potential  $V_{comb}$  of  $V_2 = 20E_R$ ,  $\epsilon = 0.25$  with  $f \approx 1.94E_R$  and:

$$(J^0, J^1, u) \approx (-0.024E_R, 0.084E_R, 0.933), \quad (21)$$

4. Potential  $V_{dw}$  of  $V_1 = 20E_R$ ,  $V_2 = 4E_R$  with  $f \approx 0.65E_R$  and:

$$(J^0, J^1, u) \approx (-1.16 \times 10^{-6}E_R, 2.5 \times 10^{-5}E_R, 0.802). \quad (22)$$

Initially the quantum state of the gas of  $N_p = \rho L$  particles is an eigenstate  $\psi_0$  of the Hamiltonian  $H$  with no interactions,  $g = 0$ . The chosen initial states is the least energy eigenstate where all the particles populate the  $p$ -band – it is a product of Bloch functions with quasimomentum  $q_*$  minimizing  $E^1(q)$ .

The subsequent evolution  $\psi(t) = \exp(-iHt/\hbar)\psi_0$  is governed by full, three-band  $H$ . The population of the  $p$ -band is given by

$$N_p(t) = \langle \psi(t) | \hat{n}_p | \psi(t) \rangle$$

Initially,  $N_p(t = 0) = \rho L$ . For  $t > 0$  the population  $N_p(t)$  drops due to interaction-driven coupling to other



bands. The temporal dependence shows some long-term oscillatory behavior that is attributed to the finiteness of the system and that of the Hilbert space. To mitigate these effects, we consider long-time average  $L_p = \overline{N_p(t)}$ .

Let us discuss the dependence of  $N_p(t)$  and  $L_p$  on the interaction strength  $g$ , that can be altered by means of Feshbach resonance [26].

The value of  $\xi = J^1/U^{1111}$  parameter indicating together with  $\rho$  the position in the phase diagram of the BH model is relatively low for  $V_{\text{latt.}}$ , of  $V_{dw}$  and at least order of magnitude larger for  $V_{na}$  or  $V_{\text{comb.}}$ . We fix  $\rho = 1.25$  to ensure that no matter the value  $\xi$ , the eigenstates of the system are the superfluid states. This ensures the probability of double-occupancy of a single site does not strongly depend on  $J/U$ . When  $\rho = 1$  and  $J/U \ll 0.3$  the gas would be a Mott-insulator single site occupation. The double-occupancy would possible only due to virtual processes the value of  $J/U$  would set the degree of stability of the gas, not the potential properties.

Under such assumptions the relative loss defined as  $\delta = (\rho L - L_p)/\rho L$  measures the depletion of the  $p$ . As revealed by a numerical simulation, for as long as  $U^{1111} \ll f$  the losses  $\delta$  for potentials  $V_{\text{latt.}}$ ,  $V_{na}$ ,  $V_{\text{comp.}}$ ,  $V_{dw}$  scale as  $\delta = A(U^{1111}/E_R)^\alpha$ . Fitting the numerical data show in Fig. 5 we find that for  $V_{\text{latt.}}$  we have  $A = 0.13900 \pm 0.00028$ ,  $\alpha = 1.83090 \pm 0.00039$ ; for  $V_{na}$  we have  $A = 0.28983 \pm 0.00042$ ,  $\alpha = 1.92133 \pm 0.00028$ ; for  $V_{\text{comb.}}$  we have  $A = 0.083270 \pm 9.0 \cdot 10^{-5}$ ,  $\alpha = 1.94114 \pm 0.00020$ ; for  $V_{dw}$  we have  $A = 0.94703 \pm 0.00054$ ,  $\alpha = 1.97562 \pm 0.00011$ . The fittings, as evident from Fig. 5 differ mainly by the prefactor, with losses for the  $V_{\text{comb.}}$  being smaller with respect to the  $V_{\text{latt.}}$  by approximately 30% for same value of  $U^{1111}$ . Together with order of magnitude larger  $J^1$  potential  $V_{\text{comb.}}$  provides a compelling way to realize a weakly interacting  $p$ -band superfluid.

#### IV. RESONANT COUPLING OF $S$ -BAND TO $P$ -BAND

##### A. Synthetic ladder

Coupling of the  $s$  and  $p$  bands can be achieved by a periodic modulation of the system with the frequency  $\omega = \bar{E}^1 - \bar{E}^0$  (see [12–14, 19]). The modulation considered in this work is by shifting of the position of the lattice:

$$V(x, t) = V(x - A \sin \omega t).$$

The potential oscillation implies a co-movement of the instantaneous Wannier functions:

$$\mathcal{W}_n^\alpha(x, t) = \mathcal{W}_n^\alpha(x - A \sin \omega t)$$

For fixed  $t$  the Hamiltonian (1), in the basis set by  $\mathcal{W}_i^\alpha(x, t)$ , will take the form of  $H_{\text{MBH}}$  with time-independent coefficients. Nevertheless, correctly derived

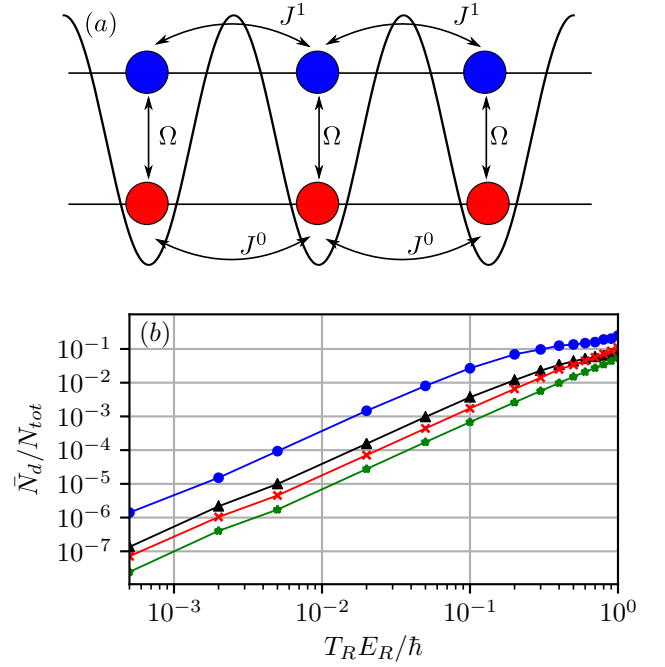


Figure 6. Mean losses from  $s - p$  band, noninteracting ladder system measured as  $\bar{N}_d$  population as a function of  $T_R$  – Rabi frequency oscillation between  $s$  and  $p$  band (see text). Black triangles, red crosses, blue circles, green stars show losses for  $V_{\text{latt.}}$ ,  $V_{na}$ ,  $V_{dw}$ ,  $V_{\text{comb.}}$  lattices, for ( $V_x = 30E_R$ ,  $\epsilon = 0.1$ ,  $V_1 = 20E_R$  and  $V_2 = 4E_R$ ,  $V_1 = 20E_R$  and  $\epsilon = 0.25$  respectively).

time-evolution equation of motion, has to take into the account the time-dependence of the basis. The resulting Time dependent Schrödinger equation is of the form [14, 45]:

$$\partial_t \psi = H_{\text{MBH}} \psi - \sum_i \sum_{\alpha, \beta} \mathcal{T}_{ii}^{\alpha\beta} (a_i^\alpha)^\dagger a_i^\beta \psi A \omega \cos \omega t. \quad (23)$$

The extra terms proportional to  $\mathcal{T}_{nm}^{\alpha\beta}$  do not couple within the same band as  $\forall m, n : \mathcal{T}_{nm}^{\alpha\alpha} = 0$ . If the potential is symmetric with respect to the middle of the unit cell, the coefficients  $\mathcal{T}_{ii}^{\alpha\beta} = 0$ ,  $\alpha + \beta \equiv 0 \pmod{2}$ , and they couple just bands of opposite parity, for example  $s$  and  $p$  band, but also  $p$  to the  $d$  band.

A 1D optical system, where just the  $s$  and  $p$  bands are to be populated can be seen as a two leg ladder system [see Fig. 6(a)] This construction shares many features with the synthetic dimension construction where the confined dimension can be mapped to populating two or more atomic states [46], in particular that ladder sites that are separated just in the synthetic dimension are physically in the same place, which allows for strong interactions between the two ladder legs. The hoppings along the each of the lattice legs is governed by  $J^0$  and  $J^1$  respectively, possibly allowing to implement complex ladder systems such as [33].

With no interaction, such a effective single particle sys-

tem decomposes into fixed quasimomentum sectors:

$$i\hbar\partial_t \begin{pmatrix} \psi_k^0 \\ \psi_k^1 \end{pmatrix} = H_{\text{ladd}} \begin{pmatrix} \psi_k^0 \\ \psi_k^1 \end{pmatrix}, \quad (24)$$

where:

$$H_{\text{ladd}} = \begin{pmatrix} E^0(k) & iT^{01}A\omega \cos(\omega t) \\ -iT^{01}A\omega \cos(\omega t) & E^1(k) \end{pmatrix}.$$

By transforming to a rotating frame  $(\psi_k^0 e^{i\delta_0 t}, \psi_k^1 e^{i\delta_1 t})$  and using the RWA, the equation of motion becomes time-independent, when  $\delta_2 - \delta_1 = \omega$ :

$$i\hbar\partial_t \begin{pmatrix} \psi_k^0 \\ \psi_k^1 \end{pmatrix} = H_{\text{ladd,RWA}} \begin{pmatrix} \psi_k^0 \\ \psi_k^1 \end{pmatrix}, \quad \Omega = T^{01}A\omega, \quad (25)$$

where

$$H_{\text{ladd,RWA}} = \begin{pmatrix} E^0(k) - \hbar\delta_0 & \Omega \\ \Omega & E^1(k) - \hbar\delta_1 \end{pmatrix}. \quad (26)$$

When  $\delta_i \approx E^i(k)$ , the Rabi oscillations frequency is  $\Omega = T^{01}A\omega$ . For  $\Omega$  dominating the bandwidths  $\Delta E^i$  this behavior is  $k$ -independent. As a result, any initial state prepared in one of the ladder legs oscillates between the two legs. The Rabi oscillations are further distorted in the presence of the interaction.

When coupling to other bands beyond  $s$  and  $p$  cannot be neglected, system fails to be modeled by a two-leg ladder. This deviation from the ladder system is again measured by mean occupation of  $d$  and higher bands,  $\delta = \bar{N}_{\geq d}/N_{\text{tot}}$ . Depletion is possible also by means of the interaction.

## B. Realization in different potentials

In this section we compare the simulations of the two-band ladder for the in the 4 potentials discussed this article.

The Hamiltonian form used for the describing the movement of the particles in the ladder, after truncating to the  $s$  and  $p$  bands takes the form:

$$H_L = -J^0 \sum_{n=1}^L (a_n^0)^\dagger a_{n+1}^0 - J^1 \sum_{n=1}^L (a_n^1)^\dagger a_{n+1}^1 + H. \quad (27)$$

$$+ iT^{01}A\omega (a_n^0)^\dagger a_{n+1}^1 \cos \omega t + H.c. + H_{\text{int.}}, \quad (28)$$

where

$$H_{\text{int}} = \sum_n \frac{U_{nnnn}^{\alpha\beta\gamma\delta}}{2} \sum_{\alpha,\beta,\gamma,\delta=0,1} (a_i^\alpha)^\dagger (a_i^\beta)^\dagger a_i^\gamma a_i^\delta. \quad (29)$$

To meaningfully compare the four potentials pick the same realizations in the Section III. In addition to parameter values given in Eqs. (19)-(22),

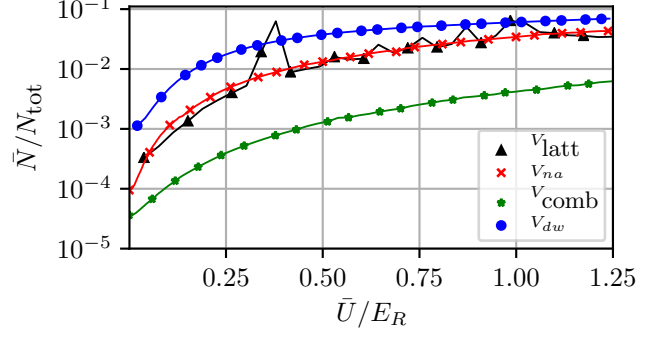


Figure 7. Depletion of the  $s, p$  band by as a function of  $\bar{U} = (U^{0000} + U^{1111})/2$  for such an oscillation amplitude that corresponds to  $T_R E_R / \hbar = 0.02$  in Fig. 6. At  $\bar{U} = 0$  the depletion is finite and solely due to off-resonant coupling of  $s, p$  band to higher  $d$  band. Increase of the interaction results in further depletion of  $s, p$  band. The legend identifies the four potential discussed in the main text. The  $V_{\text{comb}}$  potential is characterized by losses smaller for large interaction approximately by an order of magnitude, despite much larger hopping values.

we have that for  $V_{\text{latt}}, V_{na}, V_{\text{comb}}, V_{dw}$  the  $T^{01} \approx 1.57E_R, 0.85E_R, 0.77E_R, 0.86E_R$  respectively.

We opt to compare the ladder depletion in the four potentials when all in all four cases the Rabi oscillation period  $T_R$  takes the same value. Ordinarily  $T_R = 2\pi/\Omega$  with  $\Omega = |T^{01}A\omega|$ . When coupling to the  $d$  band is included and becomes significant, the system does not undergo pure Rabi oscillation. More complicated oscillation pattern emerges. We define  $T_R$  for each amplitude of modulation by fitting the  $A + B \sin(t/T_R)$  to the temporal dependence of  $N_s(t)$ .

First we consider short ladder of total length  $L = 4$ . We initialize the evolution with a quasimomentum  $k = 0$  state  $\psi_0$  in the  $s$ -band, By fixing initial  $k$  allows consider  $\Omega$  smaller than the bandwidth and still observe model Rabi oscillations, by setting  $\omega = E^1(k=0) - E^0(k=0)$ . As pictured in Fig. (6), the losses measured by  $\bar{N}_d$ , in the limit of small  $T_R$  scale as  $\bar{N}_d = A(T_R)^\alpha$ . For the four potentials we find that :  $\bar{N}_{d,\text{latt}} = (0.277 \pm 0.026)T_R^{1.895 \pm 0.023}$ ,  $\bar{N}_{d,na} = (0.121 \pm 0.013)T_R^{1.895 \pm 0.023}$ ,  $\bar{N}_{d,\text{comb}} = (0.0480 \pm 0.0057)T_R^{1.901 \pm 0.025}$ ,  $\bar{N}_{d,dw} = (2.92 \pm 0.11)T_R^{1.9550 \pm 0.0079}$ . This scaling applies when  $\bar{N}_d \ll 1$ , In all cases we find that  $\bar{N}_{d,\text{comb}}$ , are approximately an order of magnitude smaller than  $\bar{N}_{d,\text{latt}}$ , with  $\bar{N}_{d,na}$ , being in between. The losses for the double-well are order of magnitude larger than for the remaining systems. This is because of the lowest value of  $f \approx 0.65E_R$  out of the four samples.

If the modulated system is also interacting an interesting interplay of shaking and interaction may occur. To simulate such a case we consider the same four potentials, modulated with a modulation amplitude  $A$  such that the noninteracting Rabi oscillation period  $T_R = 0.02\hbar/E_R$ .

The Fig. 6) shows the dependence of the  $\bar{N}_d$  on the



mean interaction strength  $\bar{U} = (U^{0000} + U^{1111})/2$  (see also (19)-(22)). The interaction strength would be tuned with use of the Feshbach resonance, thus scaling both  $U^{1111}, U^{0000}$  by a common factor. For  $\bar{U} = 0$  the results from Fig. 7 are reproduced, in particular  $\bar{N}_d$  is finite. For increasing  $\bar{U} > 0$  for each of the four potentials the interaction causes the additional losses on top of the modulation losses. It is evident that the losses for the  $V_{\text{comb}}$  potential grow slowest with the  $\bar{U}$ . This is due to the combination of factors: first it allows to reach high anharmonic band placement (large value of  $f \approx 2E_R$ ), second as evident from Fig. 4 the value of  $|U^{1102}/\bar{U}|$  is relatively small compared to other potentials 0.17, 0.32, 0.11, 0.23 for  $V_{\text{latt}}, V_{na}, V_{\text{comb}}, V_{dw}$ . This means that if  $\bar{U}$  is fixed to a given value, then the terms responsible for interaction-driven losses come with a smaller prefactor than in the other potentials. This advantage together with largest value of  $f$  (which affects also modulation) allows to observe order of magnitude smaller depletion of the  $s, p$  band system. This also explains why the difference in stability is for  $\bar{U} \neq 0$ ,

## V. CONCLUSIONS AND OUTLOOKS

The subwavelength comb potential makes it possible to implement potentials that break the constraints implied by the diffraction limit put on constructions based on the AC-Stark effects. We have constructed lattice potentials with anharmonic potential wells, that can be realistically implemented in laboratory. The anharmonicity enhances the stability of the  $p$ -band gas, and allows to couple just two optical band lattices, in our case lowest energy  $s$  and  $p$  band. The latter was presented by implementing a synthetic dimension  $s - p$  band ladder.

Another important feature of the constructed potentials is the ability to preserve large value of the hopping rate.

The remaining open question is the applicability of the construction for the interacting bosonic systems. A fundamental problem is description of interaction-driven depletion of dark states, and a choice of a proper atom species that would allow the  $\Lambda$  system construction in for an collisionally interacting ultracold atom gas.

## ACKNOWLEDGMENTS

This work has been supported by National Science Centre project 2016/23/D/ST2/00721 and in part by PL-Grid Infrastructure (prometheus cluster).

- 
- [1] D. Jaksch, C. Bruder, J. I. Cirac, C. W. Gardiner, and P. Zoller, Physical Review Letters **81**, 3108 (1998).
  - [2] M. Greiner, O. Mandel, T. Esslinger, T. W. Hänsch, and I. Bloch, nature **415**, 39 (2002).
  - [3] M. Lewenstein, A. Sanpera, and V. Ahufinger, *Ultracold Atoms in Optical Lattices: Simulating quantum many-body systems* (Oxford University Press, 2012).
  - [4] T. Müller, S. Fölling, A. Widera, and I. Bloch, Physical review letters **99**, 200405 (2007).
  - [5] G. Wirth, M. Ölschläger, and A. Hemmerich, Nature Physics **7**, 147 (2011).
  - [6] X. Li, Z. Zhang, and W. V. Liu, Physical review letters **108**, 175302 (2012).
  - [7] T. Sowiński, M. Łącki, O. Dutta, J. Pietraszewicz, P. Sierant, M. Gajda, J. Zakrzewski, and M. Lewenstein, Physical review letters **111**, 215302 (2013).
  - [8] P. Hauke, E. Zhao, K. Goyal, I. H. Deutsch, W. V. Liu, and M. Lewenstein, Physical Review A **84**, 051603 (2011).
  - [9] M. Ölschläger, T. Kock, G. Wirth, A. Ewerbeck, C. M. Smith, and A. Hemmerich, New Journal of Physics **15**, 083041 (2013).
  - [10] C. Wu, Physical review letters **101**, 186807 (2008).
  - [11] M. Zhang, H.-h. Hung, C. Zhang, and C. Wu, Physical Review A **83**, 023615 (2011).
  - [12] N. Gemelke, E. Sarajlic, Y. Bidel, S. Hong, and S. Chu, Physical review letters **95**, 170404 (2005).
  - [13] T. Sowiński, Physical review letters **108**, 165301 (2012).
  - [14] M. Łącki and J. Zakrzewski, Physical review letters **110**, 065301 (2013).
  - [15] X. Zhou, S. Jin, and J. Schmiedmayer, New Journal of Physics **20**, 055005 (2018).
  - [16] M. Köhl, H. Moritz, T. Stöferle, K. Günter, and T. Esslinger, Physical review letters **94**, 080403 (2005).
  - [17] D. Hu, L. Niu, B. Yang, X. Chen, B. Wu, H. Xiong, and X. Zhou, Physical Review A **92**, 043614 (2015).
  - [18] L. Niu, S. Jin, X. Chen, X. Li, and X. Zhou, Physical review letters **121**, 265301 (2018).
  - [19] C. Cabrera-Gutiérrez, E. Michon, M. Arnal, G. Chatelain, V. Brunaud, T. Kawalec, J. Billy, and D. Guéry-Odelin, The European Physical Journal D **73**, 170 (2019).
  - [20] C. Sträter and A. Eckardt, Physical Review A **91**, 053602 (2015).
  - [21] A. Kastberg, W. D. Phillips, S. Rolston, R. Spreuw, and P. S. Jessen, Physical review letters **74**, 1542 (1995).
  - [22] A. Isacsson and S. Girvin, Physical Review A **72**, 053604 (2005).
  - [23] M. Łącki, M. Baranov, H. Pichler, and P. Zoller, Physical review letters **117**, 233001 (2016).
  - [24] Y. Wang, S. Subhankar, P. Bienias, M. Łącki, T.-C. Tsui, M. A. Baranov, A. V. Gorshkov, P. Zoller, J. V. Porto, S. L. Rolston, *et al.*, Physical review letters **120**, 083601 (2018).
  - [25] J. Budich, A. Elben, M. Łącki, A. Sterdyniak, M. Baranov, and P. Zoller, Physical Review A **95**, 043632 (2017).
  - [26] C. Chin, R. Grimm, P. Julienne, and E. Tiesinga, Reviews of Modern Physics **82**, 1225 (2010).
  - [27] W. Kohn, Physical Review **115**, 809 (1959).

- [28] S. Kivelson, *Physical Review B* **26**, 4269 (1982).
- [29] N. Marzari, A. A. Mostofi, J. R. Yates, I. Souza, and D. Vanderbilt, *Reviews of Modern Physics* **84**, 1419 (2012).
- [30] M. P. Fisher, P. B. Weichman, G. Grinstein, and D. S. Fisher, *Physical Review B* **40**, 546 (1989).
- [31] T. Stöferle, H. Moritz, C. Schori, M. Köhl, and T. Esslinger, *Physical review letters* **92**, 130403 (2004).
- [32] J. Zakrzewski and D. Delande, in *AIP Conference Proceedings*, Vol. 1076 (American Institute of Physics, 2008) pp. 292–300.
- [33] X. Li, E. Zhao, and W. V. Liu, *Physical Review A* **83**, 063626 (2011).
- [34] M. Mark, E. Haller, K. Lauber, J. Danzl, A. Daley, and H.-C. Nägerl, *Physical review letters* **107**, 175301 (2011).
- [35] M. Lacki, P. Zoller, and M. Baranov, *Physical Review A* **100**, 033610 (2019).
- [36] V. Boyer, R. Godun, G. Smirne, D. Cassettari, C. Chandrashekar, A. Deb, Z. Laczik, and C. Foot, *Physical Review A* **73**, 031402 (2006).
- [37] J. Liang, R. N. Kohn Jr, M. F. Becker, and D. J. Heinzen, *Applied optics* **49**, 1323 (2010).
- [38] D. Bowman, P. Ireland, G. D. Bruce, and D. Cassettari, *Optics Express* **23**, 8365 (2015).
- [39] A. Görlitz, T. Kinoshita, T. Hänsch, and A. Hemmerich, *Physical Review A* **64**, 011401 (2001).
- [40] M. Anderlini, J. Sebby-Strabley, J. Kruse, J. V. Porto, and W. D. Phillips, *Journal of Physics B: Atomic, Molecular and Optical Physics* **39**, S199 (2006).
- [41] V. M. Stojanović, C. Wu, W. V. Liu, and S. D. Sarma, *Physical review letters* **101**, 125301 (2008).
- [42] P. Lee, M. Anderlini, B. Brown, J. Sebby-Strabley, W. Phillips, and J. Porto, *Physical Review Letters* **99**, 020402 (2007).
- [43] J. Sebby-Strabley, M. Anderlini, P. S. Jessen, and J. V. Porto, *Physical Review A* **73**, 033605 (2006).
- [44] M. Anderlini, P. J. Lee, B. L. Brown, J. Sebby-Strabley, W. D. Phillips, and J. V. Porto, *Nature* **448**, 452 (2007).
- [45] H. Pichler, J. Schachenmayer, A. J. Daley, and P. Zoller, *Physical Review A* **87**, 033606 (2013).
- [46] A. Celi, P. Massignan, J. Ruseckas, N. Goldman, I. B. Spielman, G. Juzeliūnas, and M. Lewenstein, *Physical review letters* **112**, 043001 (2014).